Article

Experimental Study on Performance of Steel Fiber-Reinforced Concrete V-Shaped Columns

Rafea F. Hassan [1] , **Nabeel H. Al-Salim** [1] **, Nisreen S. Mohammed** [2] **and Husam H. Hussein** [3,*]

1   Civil Engineering Department, College of Engineering, University of Babylon, Babylon, Iraq;
    eng.rafea.flaih@uobabylon.edu.iq (R.F.H.); eng.nabeel.hasan@uobabylon.edu.iq (N.H.A.-S.)
2   Civil Engineering Department, University of Technology, Baghdad, Iraq; 40055@uotechnology.edu.iq
3   Department of Civil Engineering, Ohio University, Athens, OH 45701, USA
*   Correspondence: hh236310@ohio.edu

Abstract: Structural engineers have used V-shaped columns based on technical requirements. The inclination of the V-shaped column underlines the individual purpose of the base floor. However, there is no any specification or guidance on the design of V-shaped columns to date. The aim of this study is to investigate the behavior of V-shaped reinforced concrete columns with three angles between columns (30°, 60°, and 90°) in order for the results to be used in the design and analysis of the V-shaped column. The impact of using a 1.5% dosage of micro-straight-steel fiber (MSSF) in the concrete mixture was also studied. The results showed that the V-shaped column with 30°, regardless of the concrete type (with and without MSSFs), exhibited crushing at legends when the sample reached the ultimate load, while no cracks occurred at the legends during the test for the other V-shaped columns. Upon increasing the angle of inclination of the V-shaped columns, the ultimate load capacity was decreased by 24%, 23%, and 20% for V-shaped columns with 30°, 60°, and 90° angles of inclination, respectively. The addition of MSSFs in the concrete significantly improved the ultimate axial load and the bending moment compared to the reference specimens with the normal reinforced concrete (NRC). The steel-fiber-reinforced concrete (SFRC) vertical column specimen demonstrated the highest increase in axial load, and the other SFRC V-shaped and flexural specimens showed a minor increase compared to the NRC specimens.

Keywords: V-shaped column; steel fiber reinforced concrete; P–M diagram; reinforced concrete; column

1. Introduction

In recent years, the intensity in the design of buildings and bridges has been vast, and several new types of structures have appeared and were utilized. One of the new structure types is V-shaped columns [1–4]. The main advantages of the V-shaped column are that the middle span is short, and the three spans are supported by the assemblage two columns at one foundation. The V-shaped column design generally requires more steel reinforcement than the equivalent straight column, so it is very significant to improve the tensile strength of concrete. The concrete tensile strength of structural members may also be enhanced by utilizing additional steel-reinforced rebar and mixing fibers with concrete materials [5–7]. Fiber-reinforced concrete (FRC) is defined as concrete that includes short and discontinuous fibers and traditional components. Using steel fibers in concrete elements delays crack propagation, improving concrete strength and post-cracking performance [5]. This use enhances the behavior of steel-fiber-reinforced concrete (SFRC) beams in terms of load-bearing capacity, energy dissipation ability, deformation, residual stiffness, and cracking performance. Another study shows that steel-fiber-reinforced concrete beams significantly improved after cracking [6]. On the other hand, the inclusion of steel fibers in concrete components may improve the ductility rather than the concrete strengths [7].

Structural engineers used V-shaped columns based on technical requirements. The inclination of the V-shaped column underlines the individual purpose of the base floor. Two

rows of columns are provided to the superior floors, transferring all the loads to the base floor. The upper connection of the V-shaped column can exist using different approaches: with eccentric support, with a cantilever, or forked. The efficiency of a V-shaped column structure depends on the angle of inclination, the strength of the construction materials, the rigidity of the base hinges, and the frame that connected the ends to prevent displacement of the V-shaped frame [8]. To improve the performance of the V-shaped columns, FRC could be used, due to its several benefits for the characteristics of concrete materials. The FRC could be described as a composite material composed of mixes of appropriate cement fibers that improve its structural integrity [8–13]. Azzawi and Abolmaail [14] tested nine specimens to investigate the impact of steel fiber on the behavior of FRC hollow columns. It was found that the addition of steel fiber enhanced the performance of FRC hollow columns. Ikponmwosa and Salau [15] conducted an experimental test to study the effect of the micro-steel fiber on the structural performance of lateraled concrete columns. Results showed that the first crack load, ultimate strength, and ductility were enhanced by adding 1.5% steel fiber dosage to the concrete columns.

Al-Tikrite and Hadi [16] examined the impact on the behavior of reactive powder concrete circular columns, adding micro-straight, macro-deformed, waste-industrial hybridization, and waste steel fibers under axial and flexural loadings. The results showed that the ultimate axial loads were significantly enhanced by adding steel fibers, mainly in the micro-straight steel fiber. In addition, the micro-straight steel fiber could improve the behavior of the reactive powder concrete under various loading states. Yia and Lia [17] conducted experimental and analytical research to examine the seismic performance of inclined columns on a 1/20 scaled bridge model with a Y-shaped column. The bending moment was the most important factor that affected concrete cracks at the lower Y-shaped columns, while the shear stress had an insignificant influence on the damage to Y-shaped columns. To study the effect of steel fibers on the behavior of eccentrically loaded L-shaped columns, Tokgoz and Dundar [18] presented an experimental program by constructing and testing 16 L-shaped plain and steel fiber columns with a hooked steel-fiber content (39, 58, and 78 kg/m^3). The test results proved that using steel fibers in concrete affects the structural behavior of the L-shaped reinforced concrete subjected to axial and biaxial loads.

The structural columns influence the configuration of the buildings and furniture arrangement in conventional building construction, requiring columns with particular shapes. The impacts on the seismic performance of the building that incorporates these columns of concrete strength, ratios of reinforcement and axial compression have been explored. Teng et al. [19] tested a two-span with column frames under seismic load. The researchers also utilized a finite-element program that led to the production of a load vs. displacement curve, peak load, coefficient of ductility, energy dissipation capacity, and stiffness curve degradation for the specially shaped column frame. Studies by [20,21] presented an experimental investigation of the seismic behavior of L-shaped columns. The proportion of axial compression and stirrup space impact-bearing capability, failure mode, and deformation ductility were examined based on tests on six L-shaped RC columns reinforced by steel bars. The findings reveal that samples with a lower axial load and high stirrup properties values are higher in terms of ductility and seismic efficiency. In contrast, samples with a smaller axial load or small stirrup properties values were lower in ductility and seismic efficiency. Lomiento et al. [1] provided an overview of the capacity of V-shaped bridge bents. The evaluation of two V-shaped RC bridge bents flexural and shear capacities was verified against experimental findings from 1:3-scale tests samples. A computational technique dependent on incremental analysis that considers the vertical load variability in the columns of the bents produces a reasonable estimate of the general bent performance.

Accordingly, the use of steel fiber as an additional material in concrete components improves the overall performance of the concrete mechanical properties. However, there is no specification and guidance on designing a V-shape column for micro-straight steel-fiber (MSSF)-reinforced concrete. To design the V-shaped column, understanding the behavior of V-shaped reinforced concrete columns, reinforced with different angles between columns,

is essential. The aim of this research is to investigate the behavior of V-shaped reinforced concrete columns with three angles between columns (30°, 60°, and 90°) in order for the results to be used in the design and analysis of the V-shaped column. The MSSF content of 1% was mixed with concrete to study the effects of MSSF on the V-shaped column performance. The V-shaped columns with cantilever ends were conducted to simulate a critical case and show the MSSF's influence. Along with V-shaped column specimens, two straight columns and two beams were also tested to study the impact of MSSF on axial compression and flexural behaviors. The vertical displacement, horizontal movement at the unrestrained tips, and relative displacement at the convergence region of the tested V-shaped column were documented at each load step, along with the first crack and failure loads.

2. Experimental Program

In this research, the flexural and compression test methods were conducted to identify the axial load and bending moment to assemble a design interaction axial load–bending moment (P–M) curve. Different angles between columns (30°, 60°, and 90°) in V-shaped specimens were used in an attempt to obtain more points for the P–M curve. It should be noted that the tests were performed on both NRC and SFRC specimens to understand the impact of MSSF on the interaction curves.

2.1. Apparatus

This section shows the dimensions and reinforcement of all specimens. Two straight columns and two beam specimens were constructed with dimensions of 10 cm × 10 cm × 70 cm and reinforcement. The beams and column were designed following the ACI code [22], and four rebars of 8 mm diameter and 5 mm diameter rebars were utilized as longitudinal reinforcement and closed stirrups spaced at 6 cm, respectively, as shown in Figure 1. Six V-shaped columns were cast to study the effect of inclination angle and MSSF on structural behavior. The base dimensions of the V-shaped column are 20 cm wide, 15 cm high, and 10 cm in depth, with inclined columns of 70 cm inner length and a square cross-section of 10 cm. In Figure 1, the angle of inclination between the two columns (θ) and the net distance from the end columns (X) are listed in Table 1. Three V-shaped specimens were normal-strength concrete (NSC), and the other three were cast with steel FRC. The Ø5 and Ø8 steel bar diameters were used as closed stirrups and longitudinal reinforcement to enforce the beams. For all V-shaped columns, two sizes of steel reinforcing deformed bars were used. Four bars of Ø8 mm were utilized as longitudinal reinforcement, and bars of 5 mm diameter with 6 cm spacing were used as closed stirrups for the inclined parts, along with the base of the V-shaped column. The main reinforcement was continued for both vertical and inclined columns and bent horizontally at both ends by 5 cm inside the column. Three horizontal stirrups were placed in the base of V-shaped columns spaced at 6 cm. The stirrups of the inclined V-shaped portion were placed perpendicularly to the longitudinal reinforcement, as shown in Figure 1.

Table 1. Specimen details.

Specimen ID	Material	Specimen Configuration	X (cm)	θ (°)
NRC-0	NSC	Column	-	-
NRC-30	NSC	V-shape-1	36	30
NRC-60	NSC	V-shape-2	70	60
NRC-90	NSC	V-shape-3	100	90
NRC-B	NSC	Beam	-	-
FRC-0	SFRC	Column	-	-
FRC-30	SFRC	V-shape-1	36	30
FRC-60	SFRC	V-shape-2	70	60
FRC-90	SFRC	V-shape-3	100	90
FRC-B	SFRC	Beam	-	-
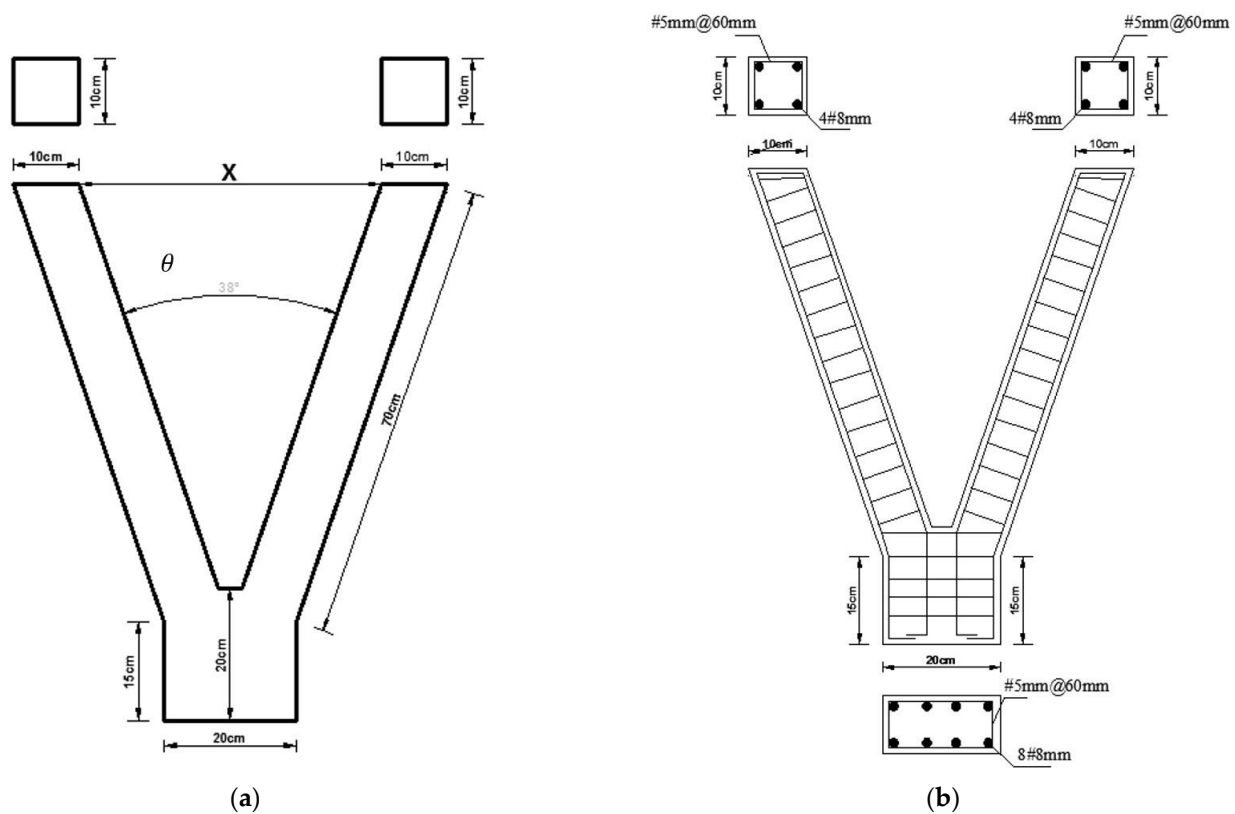
Figure 1. (**a**) Configurations of V-shaped column and (**b**) reinforcement details.

2.2. Mix Design and Materials Properties

The crushed, coarse aggregate and fine aggregate used in this study were a maximum size of 14 mm and 4.75 mm, respectively. The coarse aggregate grading was within the requirements of the specification [23]. Potable water was used for washing, casting, and curing specimens. Ordinary Portland cement was used. Based on previous research findings and recommendations, the MSSF content of 1.5% was added to the concrete mixture [15,24]. This fiber has a length of 13 mm with a nominal tensile strength of more than 2100 MPa provided by the manufacturer (see Figure 2). According to the ACI 211.1-14 [22] recommendations, the mix was created to reach 30 MPa compressive strength with a cement content of (450 kg/m^3). The water/cement ratio was (0.46) with an 8–10 cm slump. A proportion by weight (1:1.6:2.24) was found to achieve intended compressive strength at (28) days. Mixture details are listed in Table 2. For steel-reinforced bar material properties, the 712 MPa and 735 MPa ultimate strength and yield stress of 455 MPa and 424 MPa for the Ø8 and Ø5 steel bars, receptively, were found following ASTM A615 [25].
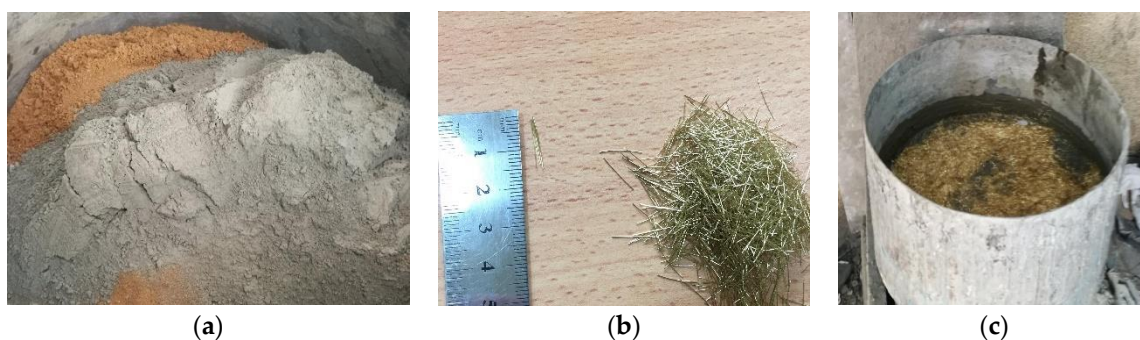

Figure 2. Concrete mix components: (**a**) sand–cement, (**b**) MSSF, and (**c**) adding fiber to mixture.

Table 2. Details of mix proportion and properties.

Materials and Properties	Amount
Mix water/cement ratio	0.46
MSSF	1.5% of specimen volume
Maximum Size Aggregate (mm)	14
Slump (cm)	8–10
Water (kg/m^3)	207
Cement (kg/m^3)	450
Fine aggregate (kg/m^3)	723
Coarse aggregate (kg/m^3)	1010

Both the NSC and steel FRC mixes were intended to obtain the intended compressive strength by maintaining a constant cement content in each mix to examine the effect of the MSSF on the concrete mechanical properties. All samples were kept in the lab until the testing date. The cubes, cylinder, and prism were tested for each mix to obtain concrete compressive strength, splitting tensile strength, and flexural strength. The concrete strength was tested for each mix in accordance with EN, B.-12390-2 [26] to estimate compressive strength at 28 days. Cubes of 150 mm were tested using a hydraulic machine with a capacity of 2500 kN, as shown in Figure 3. Splitting strength and flexural strength tests were performed, following ASTM C496/C496M-17 [27] and ASTM C78/C78M-18 [28], as shown in Figure 3. As reported in past research [24,29–31], the MSSF reduces the brittleness and increases the ductility of FRC, as listed in Table 3. In this table, brittleness ratios were calculated for both mixes by dividing the compressive to flexural strength. A high value of brittleness ratio represents a low tensile concrete capacity. Due to the use of MSSF, the brittleness ratio was decreased by 24.9%.
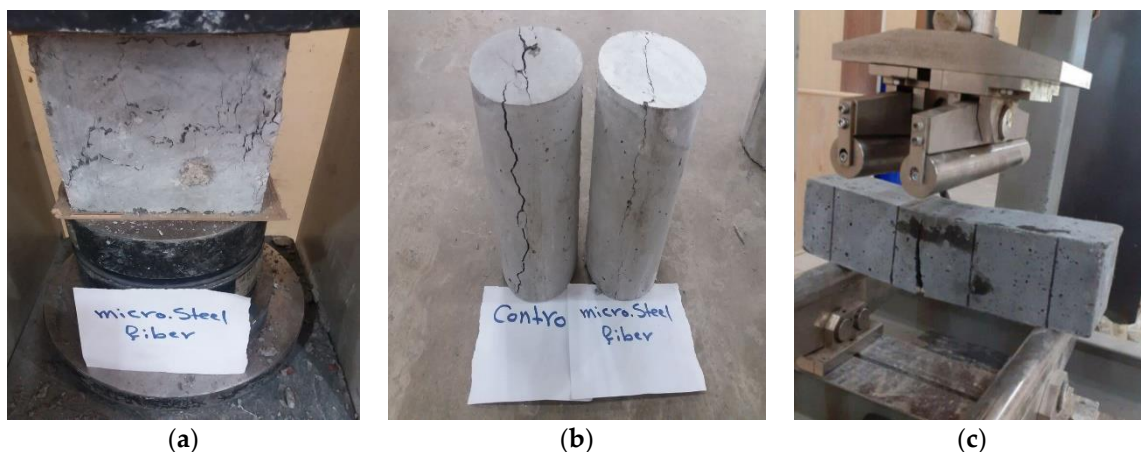
Figure 3. (**a**) Compressive strength test, (**b**) splitting strength test, and (**c**) flexural test.

Table 3. Mechanical properties of NSC and FRC mixes.

Details	Splitting Tensile (*ft*) (MPa)	Flexural Strength (*ff*) (MPa)	Compression Strength (*fcu'*) (MPa)	Brittleness Ratio
NSC	2.94	3.97	32.5	8.19
FRC	3.92	5.12	38.9	7.6

2.3. Specimen Preparation

To study the effect of MSSF and the angle of inclination on the behavior of V-shaped reinforced columns, three V-shaped columns with three different inclination angles and two straight specimens were conducted with normal reinforced concrete (NRC) and steel FRC, as shown in Figure 4. The wood molds were used to cast the specimens. The specimen casting was separated into two groups; the first group of specimens was cast with the NSC,

and the second group was cast with the FRC. An electric rotary type mixer of 0.3 m^3 capacity was used for mixing following ASTM C192/C192M [32]. To determine the mechanical properties of each batch (compressive and tensile strength), three cylinders of 100 mm × 200 mm and three cubes of 150 mm were prepared for splitting tensile strength (ASTM C496/C496M-17 [18]) and compressive strength (EN, B. (2009)-12390-2 [26]), respectively. For flexural strength, prisms of 100 mm × 100 mm × 500 mm were prepared in accordance with ASTM C78/C78M-18 [19]. To avoid forming MSSF balls through the concrete mix, the MSSF was included after all concrete components were combined to distribute the MSSF throughout the mixture. All wood molds were cleaned and oiled before putting down the reinforcement cage in the molds. The concrete was poured lightly into oiled plywood molds with three layers. After that, each specimen was shacked for 30 s using a vibrator. The specimens were wrapped with a sheet to eliminate water loss. After 24 h, the specimens were removed from the molds. Then, the specimens were submerged in the water for 28 days to finish the curing, following ASTM C192/C192M [32].

| (a) | (b) | (c) |
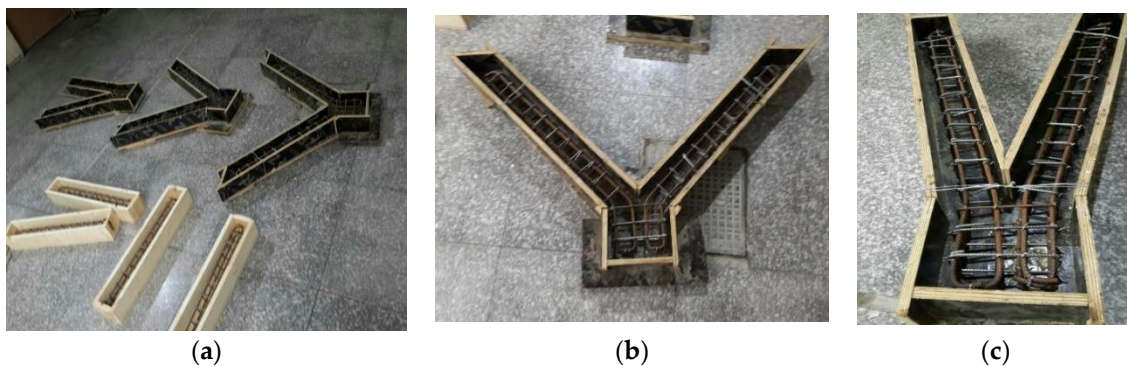
Figure 4. (**a**) All models, (**b**,**c**) details of reinforcement and details of V-shape.

2.4. Test Procedure

Ten reinforced concrete specimens, separated into three groups, were made and tested under different loading conditions to study the influence of MSSFs reinforcement and inclination angle in FRC members. Both V-shaped and straight columns were tested vertically under compression force, while two straight specimens were tested under flexure load. For the V-shaped columns, unrestrained tips were used at the ends of the inclined legs to apply a critical case. The V-shaped columns might experience the maximum moment at the connection point between the two legs in this test setup. Tests were conducted using a machine with a 400 kN testing capacity. The key attributes of the structural performance of the columns and beam specimens were identified at each loading stage during the test. A dial gauge of 0.01 mm accuracy was utilized to record the deflection at the mid-span of the beam and total displacement of vertical columns, as shown in Figure 5. For the V-shaped columns, three displacements, a vertical displacement at the inner tip point, horizontal displacement at the two inclined legs, and the relative displacement between the two inclined legs at the tip points, were measured at each step. The horizontal displacement was measured by applying two dial gages at the ends of the inclined leg at 15 cm height. An electronic vernier of 0.01 mm accuracy was fixed to the two inclined legs at 5 cm from the connection point to measure the relative displacement between the two legs.

### 2.5. Ductility and Service Stiffness

Ductility measures the material's capability to plastically deform without fracturing when subjected to different types of stresses. The ductility of vertical columns, V-shaped columns, and flexural members was determined using two methods based on two different approaches [33,34]. The first approach relies on the ratio of the deflection at 85% post the ultimate load (δu) divided by yield deflection (δy) to calculate the ductility (μ), as shown in Figure 6, which can be written as follows [35]:

$$\mu = \frac{\delta u}{\delta y} \qquad (1)$$

where μ is the ductility ratio paced on the displacement of the specimen, δy is the yield deformation, and δu is the ultimate post-deformation [36].

(**a**) (**b**) (**c**)
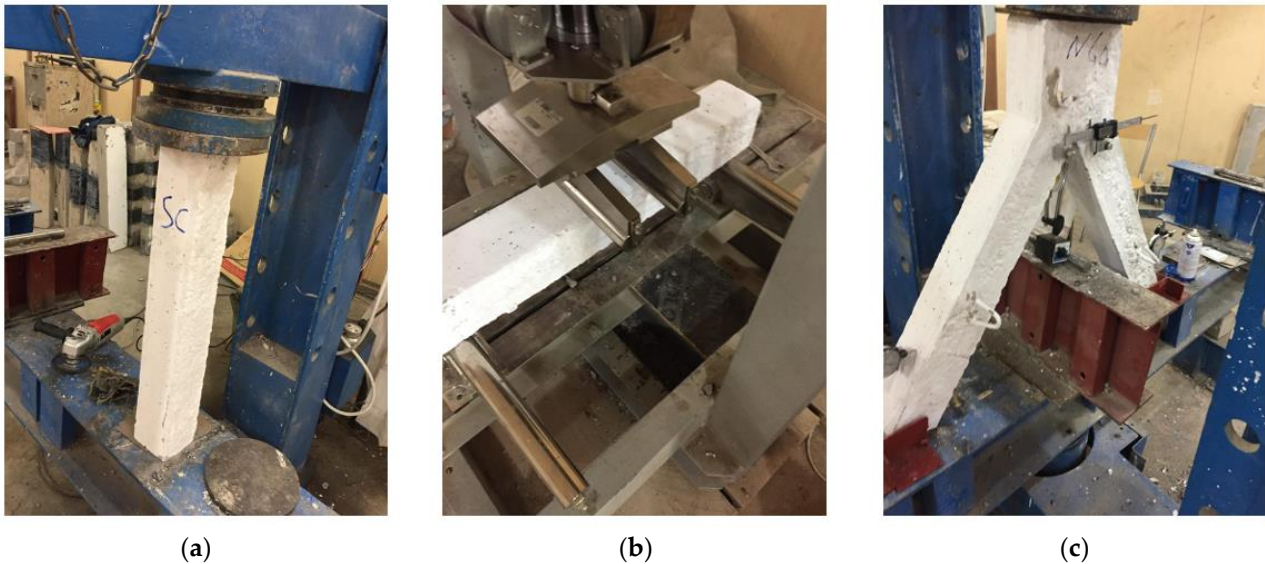
Figure 5. Test setups for (**a**) vertical column test, (**b**) beam test, (**c**) V-shaped column test.
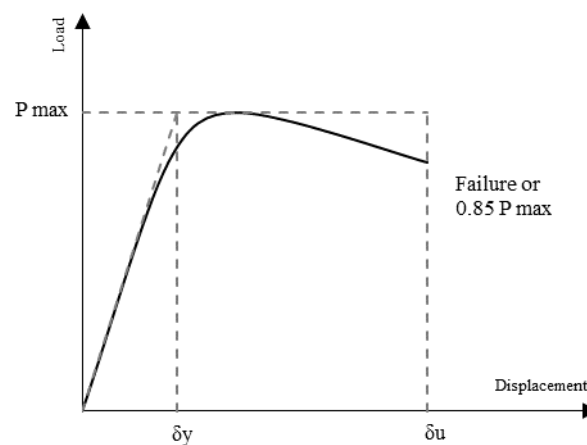
Figure 6. Determination of yield and ultimate displacements of columns, adapted from ref. [36].

The elastic deformation is determined by sketching two tangents. The 1st was tangential to the load–displacement curve and intersected the origin of the curve. The 2nd tangent was a horizontal line that traced the ultimate point in the load–displacement curve. Then, a vertical line was represented by the crossing of these tangents. The vertical line's point intersected the load–deflection curve, representing the yield point [33]. The second method used to count ductility based on energy absorption was the ratio of $A_{\delta u}$ to $A_{\delta y}$ [37].

$$\lambda = \frac{A_{\delta u}}{A_{\delta y}} \qquad (2)$$

where λ is the specimen energy absorption, $A_{\delta y}$ is the area of elastic identified under the load–displacement curve, counted from the origin to the yield load, and $A_{\delta u}$ is the area calculated from origin to the ultimate deformation up to 85% of the ultimate axial load. Depending on the state of the specimen, the initial stiffness of specimens was determined by two different approaches. The first approach is compressive stiffness, which was used for

specimens tested under a concentric load. Huo et al. [38] and Yang et al. [39] stated that the compressive stiffness is the secant stiffness matching the column strength of 0.4 ultimate loads. The second approach is flexural stiffness for specimens using the flexural test. This approach is frequently used in experimental research, where the initial stiffness is the slope of the line passing the point with 75% of the ultimate strength [40]. For the V-shaped columns, the two approaches were used to determine initial stiffness.

3. Experimental Results and Discussion

3.1. Fiber Impact on Compressive and Flexural Behaviors

3.1.1. Failure Mode

Two vertical columns with and without MSSFs were assessed under axial load. For NSC vertical column, it should be highlighted that fine cracks emerged at the top of the tested columns at load 105 kN. Upon reaching the ultimate, the column failed at 137 kN load in a brittle approach with a loud crashing sound, resulting in a sudden load drop. However, in the vertical column consisting of MSSF, tested under the same loading situations, the cracks emerged in the top of the specimen at load 140 kN, and the column failed at 187 kN load. The compressive strength of the NSC column at the first crack was 25% lower than the SFRC column, while the ultimate capacity of the NSC column was 27% lower than the SFRC column. Figure 7a shows the crack patterns of the NRC and SFRC columns, with failure at the end of the column. Due to the use of MSSF, the column did not display brittle failure. After achieving the ultimate load, the failure was slow, with a ticking sound resulting from the concrete matrix's debonding of MSSFs. The two tested columns are shown in Figure 7a.

| (a) | (b) |

Figure 7. Failure mode of NRC and FRC (**a**) columns and (**b**) beams.

For two specimens tested under flexural loading, vertical hairline cracks emerged at the tension zone at the mid-span of beams with loads of 10.5 and 18.5 kN for NSC and SFRC, respectively. With the load increase, the tension face started to crack with prorogation, while the compression face began to crush at loads of 29 and 34 kN for NSC and SFRC, respectively. The flexural strength of the NSC column at first crack was 43% lower than the SFRC column, while the ultimate capacity of the NSC column was 15% lower than the SFRC column. The failure began by crushing concrete at the compression zone at the mid-span of beams, as shown in Figure 7b. It should be noted that the crack patterns of the NSC appeared early, with wide cracks as the load increased, compared to the SFRC beam. This shows the advantage of utilizing the MSSFs in concrete mixtures.

3.1.2. Load–Displacement and Ductility Behaviors

Figure 8a depicts the axial load–axial deformation curves of the two tested columns. It was noticed that the inclusion of MSSFs positively impacted the axial load capacity of the specimen. Specifically, the addition of MSSFs in the concrete achieved the maximum increase in the load capacity under loading compared to the NSC specimen. The axial load capacity of column FRC-0 was 37% higher than the load capacity of column NRC-0. The

compressive failure strength of the NSC column was 27% lower than the SFRC column, with a lower displacement of 65%. This improvement in the column performance of the SFRC is credited to an increase in the fiber bridging the cracks. The fiber bridging influences the post-cracking compressive strength of the SFRC column. It should be highlighted that the use of MSSF affects the strength of concrete as it governs the early and post-concrete cracking [41], and the homogeneous distribution of the MSSFs throughout the matrix without interlocking between MSSFs.
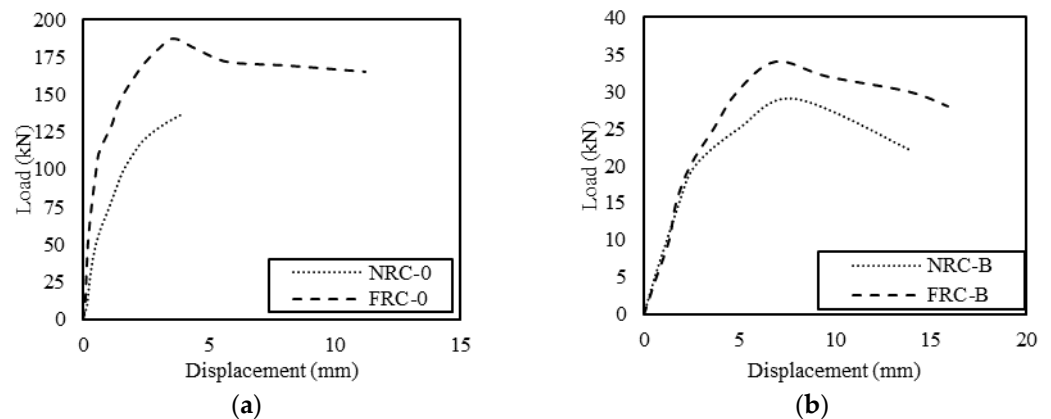
Figure 8. Load–axial deformation of NRC-0 and FRC-0 (**a**) columns and (**b**) beams.

The addition of MSSFs to concrete mix influences the post-ultimate-load behavior of the specimen tested under a concentric load by softening the descending part of the load–vertical displacement plot and avoiding sudden failure. The downward portion of the load–vertical displacement plot was due to an extra action provided by MSSFs through the bond between the MSSFs and matrix [42]. As shown above, the yield load and ultimate load increased by 27% for the SFRC column compared to the NSC column, while the corresponding axial deformation at yield load for the SFRC column was 63% lower than the NSC column. The increase in the ductility index (μ) due to the addition of MSSF was 79%, and the energy absorption (λ) increased by 78%, as shown in Table 4. Thus, the addition of MSSFs to treat the brittleness matter in the specimens under concentric load was very successful.

Table 4. Loading test results and ductility for columns and beams.

| Specimen ID	NRC-0	FRC-0	NRC-B	FRC-B
Yield load (kN)	84	115	22	27
Corresponding axial deformation at yield load (mm)	1.3	0.8	3.5	4.15
Ultimate load (kN)	137	187	29	34
Deformation at ultimate load (mm)	3.9	3.6	7.9	6.89
Post deformation at 85% post ultimate load (mm)	3.9	11.5	12.4	15.6
Ductility index (μ)	3	14.4	3.5	3.8
Energy absorption (λ)	6.5	30.2	6.1	6.5

Figure 8b depicts the load–midspan displacement curves of the tested beams. Both specimens (NRC-B and FRC-B) showed an approximately linear behavior in the ascending part of the load–deflection curve. Adding MSSF resulted in an increment in the bending capacity of 17% compared with the NRC beam, while the corresponding bending deformation at ultimate load for the SFRC beam was more than 16% that of the NSC beam. Table 4 lists the results of the beams loaded concentrically for bending under four-point loading. Adding MSSF to the flexural beams clearly softened the downward part of the

load–midspan displacement plot with an increment in the ductility index μ by 9% and the energy absorption λ by 7%.

### 3.2. Fiber Impact on V-Shaped Column Behaviors

3.2.1. Failure Mode

Figure 9 shows V-shaped columns with a 30° angle for NRC-30 and FRC-30 specimens. Figures 10 and 11 depict V-shaped columns with 60° and 90° angles, respectively. The V-shaped columns showed numerous crack patterns at various locations at the inner point of connection (tension crack), the inner face of the column leg near the connection point (tension crack), and the outer face of the column (compression crack), as shown in Figures 9–11. The failure mode of the tested V-shaped columns was dominated by the angle of inclination and occurrence of fibers. During each V-shaped column test, the development of cracks from the first crack load until failure are shown in Table 5 and Figure 5. It should be highlighted that the V-shaped column with 30°, regardless of the concrete type (with and without MSSFs), exhibited crushing at legends when the sample reached the ultimate load. The compressive strength of the NSC 30° column was 22% lower than the SFRC column at the inner point, while the ultimate capacity was 19% lower. Figure 9 shows the crack patterns of the NRC and SFRC 30° columns, where it shows the failure at the end of the column of the NSC. Due to the use of MSSF, the column did not display brittle failure. After achieving the ultimate load, the failure was slow, with a ticking sound resulting from the concrete matrix's debonding of MSSFs.

| (a) | (b) | (c) | (d) |
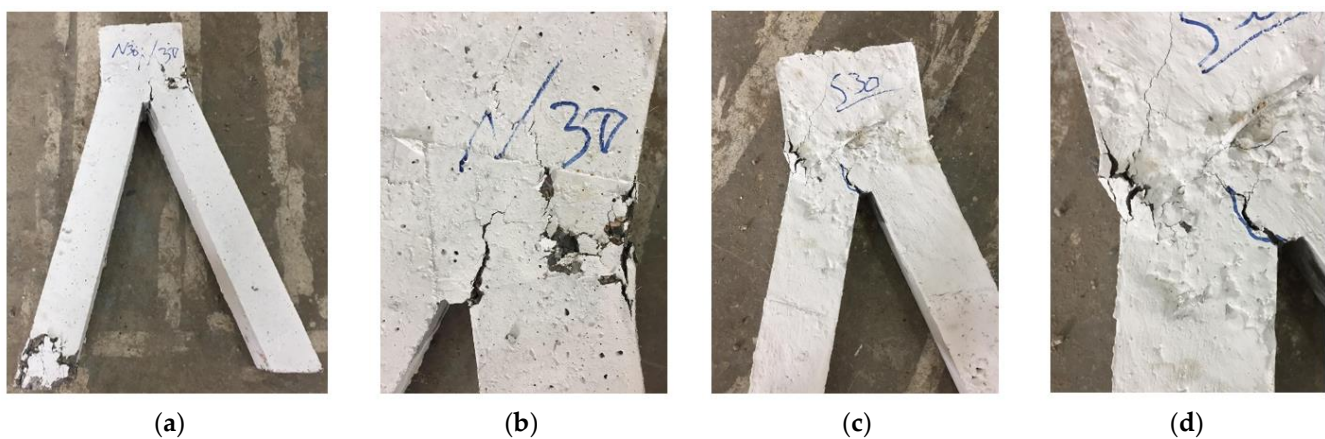
Figure 9. V-shaped columns with 30° angle (**a**) NRC-30, (**b**) NRC-30 failure zone, (**c**) FRC-30, and (**d**) FRC-30 failure zone.

| (a) | (b) | (c) | (d) |
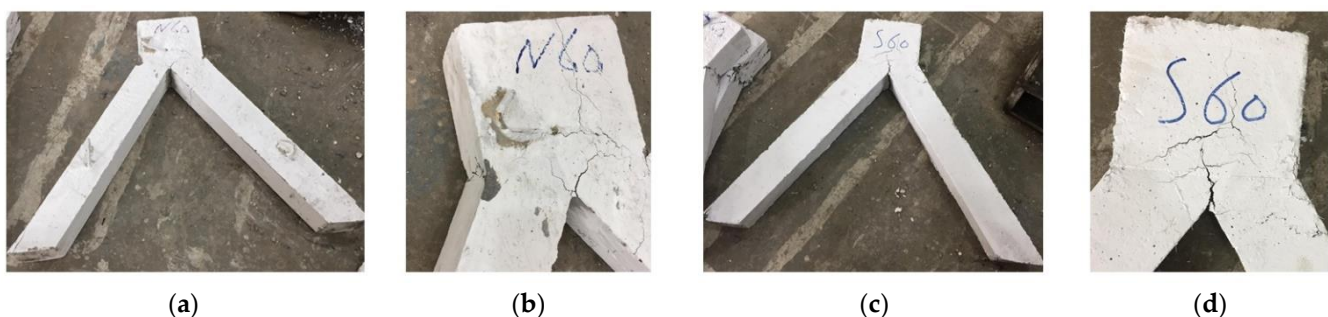
Figure 10. V-shaped columns with 60° angle (**a**) NRC-60, (**b**) NRC-60 failure zone, (**c**) FRC-60, and (**d**) FRC-60 failure zone.
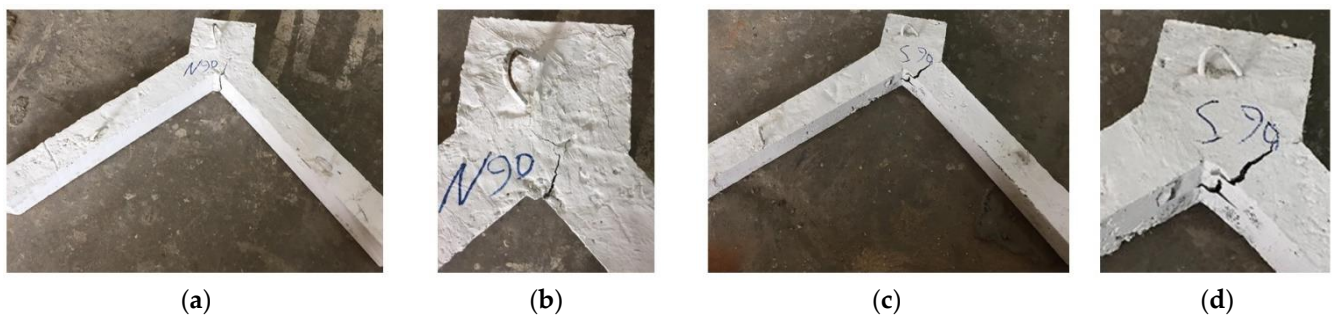
Figure 11. V-shaped columns with 90° angle (**a**) NRC-90, (**b**) NRC-90 failure zone, (**c**) FRC-90, and (**d**) FRC-90 failure zone.

Table 5. First cracking load at each location.

Specimen ID	Inner Point (kN)	Inner Face (kN)	Outer Face (kN)	Failure Load (kN)
NRC-30	142	165	175	220
NRC-60	12	30	47	70
NRC-90	5	20	Not appeared	25
FRC-30	182	213	258	272
FRC-60	28	47	58	86
FRC-90	7	12	27	30

On the other hand, no cracks occurred at the legends during the test for the other V-shaped columns. It was noted that all the V-shaped specimens showed exposure concrete crushing of the compression face at the ultimate load, excepting NRC-90 specimens, as shown in Figures 10 and 11. The V-shape columns sustained the load, even though the crack width increased as the degree of angle increased compared to NRC columns. Along with these significant cracks in the FRC, many fine cracks began due to the crack-bridging effect of MSSF. The MSSF considerably decreased the crack width of the FRC-30, FRC-60, and FRC-90 columns by 23%, 22%, and 20% compared to the NRC-30, NRC-60, and NRC-90 columns, respectively. The variation in the volume of fine cracking was affected by the tensile strength, which is impacted by the bridging effect of fiber crack.

3.2.2. Load–Displacement Behavior

The experimental load–vertical deflection, load–horizontal displacement, and load–relative displacement diagrams of the V-shaped columns with the NSC and SFRC are presented in Figures 12–14, respectively. In these figures, the ultimate load capacities of the V-shaped columns were substantially affected by the angle of inclination and inclusion of MSSF. The diagrams showed that the addition of MSSF into concrete enhances the ultimate load and ductility of the V-shaped columns. The improvement in the V-shaped column ultimate load resulting from the inclusion of MSSF was greater than the vertical columns tested under concentric load. With the inclusion of MSSFs in the V-shaped columns, the ultimate load capacity was increased by 24%, 23%, and 20% for V-shaped columns with 30°, 60°, and 90° angles of inclination, respectively. The axial load capacity of column FRC-30 was 32% higher than the load capacity of column NRC-30. The compressive failure strength of the NSC column was 19% lower than the SFRC column. This improvement is due to the fiber-bridging effect on the post-cracking compressive strength of the SFRC column.

The load–deflection curves of the NSC and SFRC columns show an elastic stage. Then, the curves gradually begin a hardening stage until the ultimate load is reached. The softening behavior occurred after the ultimate load was reached. Afterward, the load of the specimens continued the MSSF after the ultimate load dropped by 9%, 10%, and 11% for FRC-30, FRC-60, and FRC-90, respectively. At the same time, the specimens without MSSF did show a sudden drop in load–deflection curves after ultimate load. This sudden drop was due to the concrete crushing at the compression face of the columns. The load–

deflection curves of specimens with the MSSF continued to drop downward very slightly, but those without the MSSF continued to drop downward substantially.
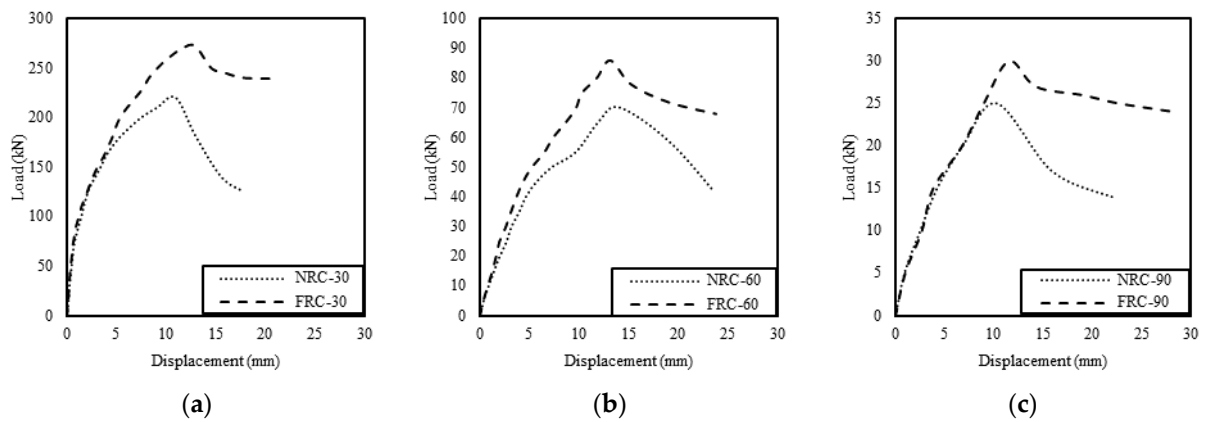

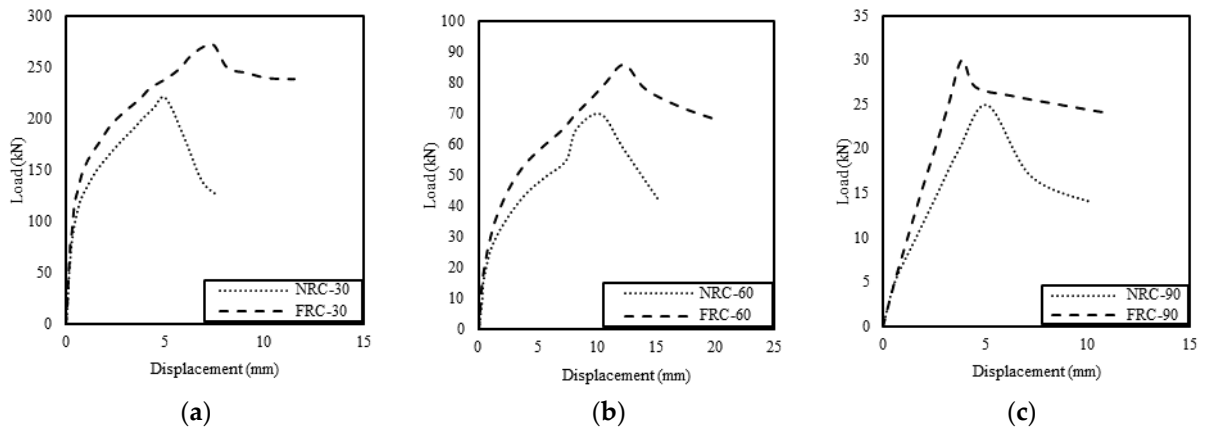**Figure 12.** Load–vertical deflection of V-shaped columns with (**a**) 30°, (**b**) 60°, and (**c**) 90° angles.

Figure 13. Load–horizontal displacement of V-shaped columns with (**a**) 30°, (**b**) 60°, and (**c**) 90° angles.
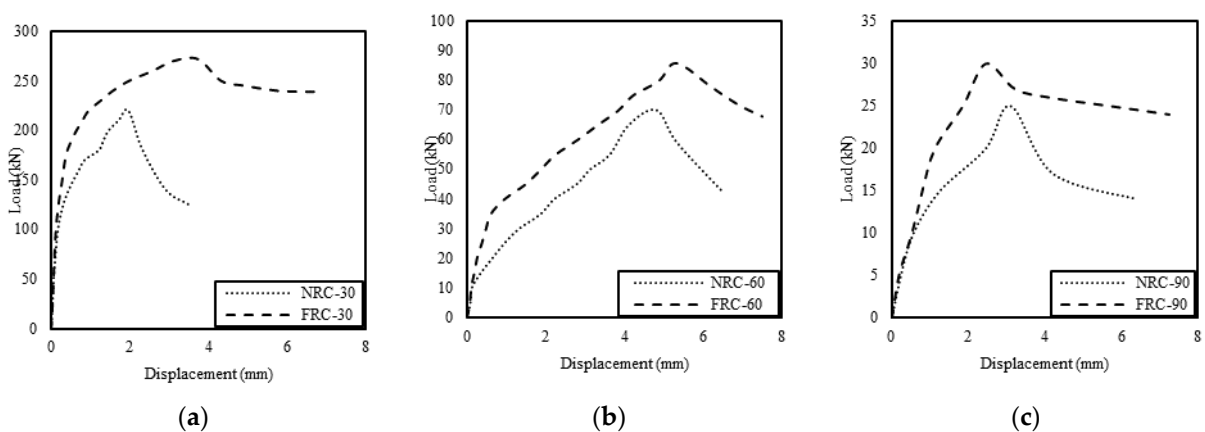

Figure 14. Load–relative displacement of V-shaped columns with (**a**) 30°, (**b**) 60°, and (**c**) 90° angles.

The horizontal and relative displacement curves for the V-shaped columns are shown in Figures 15–17, and all curves showed a semi-elastic linear response, followed by a nonlinear behavior and a drop in load capacity at failure. The values of both relative displacement and horizontal displacement at ultimate load for the V-shaped columns are listed in Table 6. The relative displacement at the ultimate load of column FRC-30 was 48% higher than the NRC-30 column, while for 60° columns, the FRC-60 column was 10%

less than the NSC-60 column. This improvement is due to the fiber-bridging effect on the post-cracking compressive strength of the SFRC column. All SFRC V-shaped columns showed increased relative and horizontal displacements at ultimate load, except the FRC-90 column. This singular behavior resulted from the main crack of the FRC-90 column, which was vertical on the inclined leg, while, for the other V-shaped columns, the main crack was vertical on the horizontal plane (see Figure 11d).
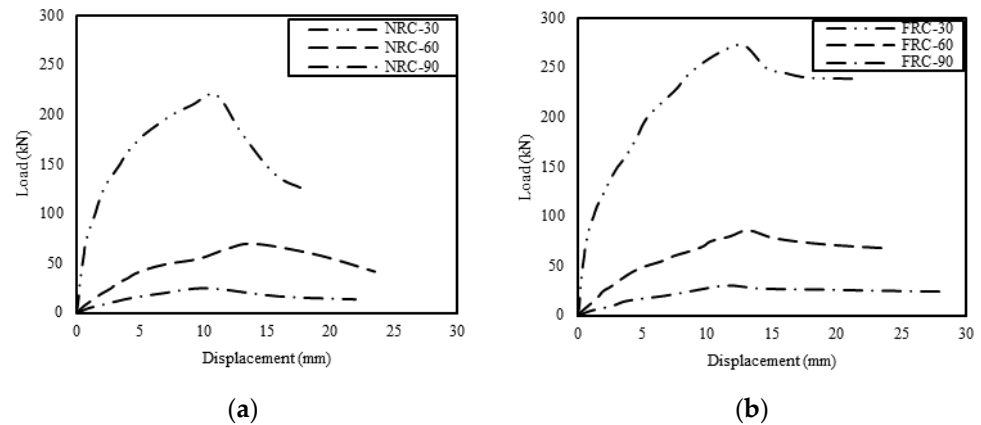
Figure 15. Load–vertical deflection comparison between V-shaped columns of (**a**) NSC and (**b**) FRC specimens.
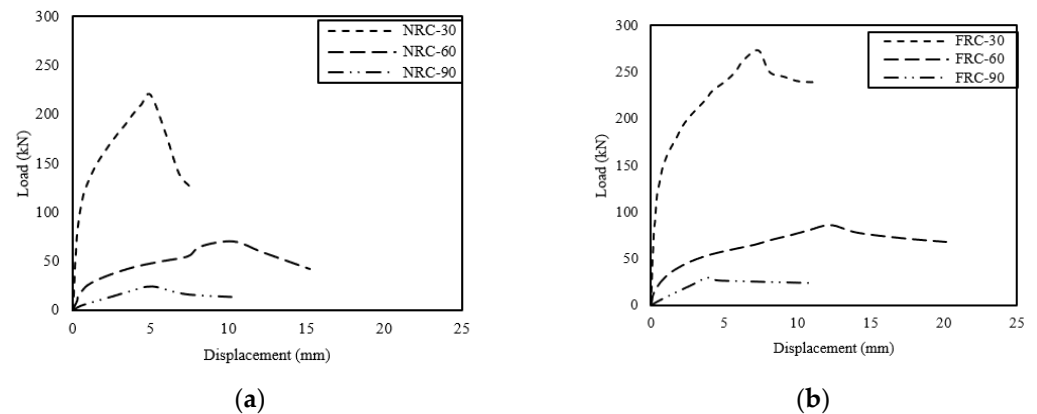
Figure 16. Load–horizontal deflection comparison between V-shaped columns of (**a**) NRC and (**b**) FRC specimens.
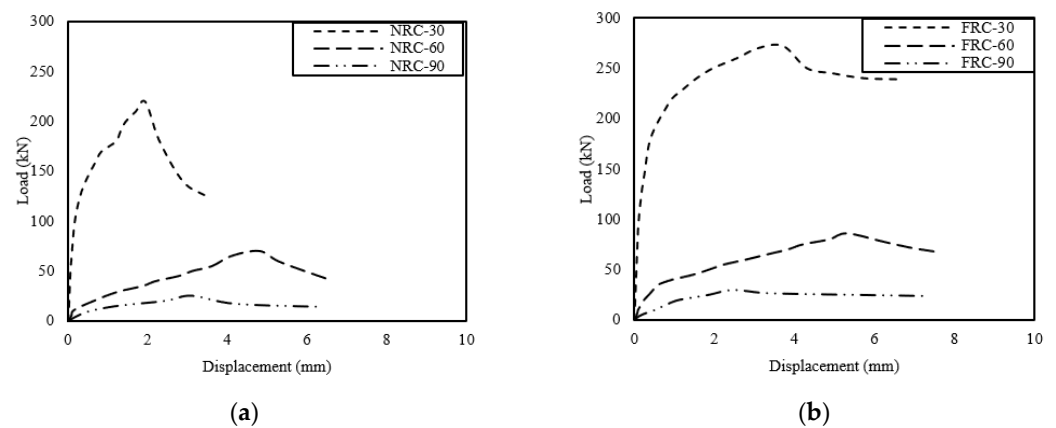

Figure 17. Load–relative deflection comparison between V-shaped columns of (**a**) NRC and (**b**) FRC specimens.

Table 6. Relative displacement and horizontal displacement at ultimate load.

Specimen ID	NRC-30	FRC-30	NRC-60	FRC-60	NRC-90	FRC-90
Relative displacement at ultimate load (mm)	1.95	3.72	4.8	5.32	3.1	2.45
Horizontal displacement at ultimate load (mm)	5.02	7.45	10.32	12.3	5.1	3.85

3.2.3. Ductility and Service Stiffness

Figure 18 and Table 7 show the influence of the inclination angle on ductility index and energy absorption. The ductility index μ and energy absorption λ significantly decreased when the angle of inclination increased. Thus, the columns of 30° show the highest ductility index and energy absorption of the V-shaped column among the other V-shaped columns, while the other columns, with larger angles, showed low ductility values. By comparing the columns with different concrete types, the results showed that the use of the MSSF significantly influences the ductility and energy absorption for all specimens.
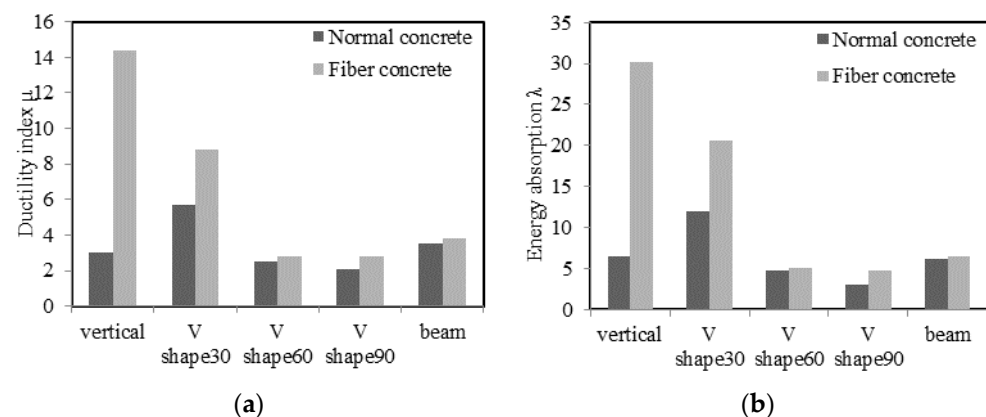
Figure 18. (**a**) Ductility index and (**b**) energy absorption of NRC and FRC specimens.

Table 7. V-shaped columns' test results and ductility.

Specimen ID	NRC-30	FRC-30	NRC-60	FRC-60	NRC-90	FRC-90
Yield load (kN)	125	135	48	59	19	21.5
Vertical deflection to yield load (mm)	2.2	2.5	7.2	6.8	6.3	7.5
Ultimate load (kN)	220	272	70	86	25	30
Vertical deflection to ultimate load (mm)	11	12.9	14	13.15	10.3	11.5
Post vertical deflection at 85% post ultimate load (mm)	12.5	22	18	19	13	21
Ductility index μ	5.7	8.8	2.5	2.8	2.1	2.8
Energy absorption λ	12	20.6	4.7	5.1	3.1	4.7

The impact of the MSSF on the values of compressive stiffness significantly decreased when the angle of inclination was increased. Therefore, the vertical columns and V-shaped columns of 30° showed the highest increase in compressive stiffness, while the other angle of inclination showed the lowest increase in the compressive stiffness. It can be noted that the NRC-60 and FRC-60 specimens have approximately the same flexural stiffness as specimens NRC-B and FRC-B. All V-shaped columns show a compressive stiffness that is higher than the flexural stiffness, as listed in Table 8.

On the other hand, the influence of the MSSF on the flexural stiffness values has a lesser effect, as shown in Table 8. The increase of 79% in compressive stiffness was observed from the vertical columns, while the compressive stiffness of the V-shaped columns with 30° and 60° angles of inclination amounted to 19% compared to the NRC specimens. The V-shaped column with a 90° angle showed the lowest percent increase in compression stiffness, of about 9.1%, due to the wide-angle at the V-shape angle. With the reduction in

tension cracks, the effect of the MSSF was more noticeable. Therefore, the presence of the MSSF in the concrete leads to higher compressive stiffness.

Table 8. Compressive stiffness and flexural stiffness of specimens.

Specimen ID	Compression Stiffness Kc (kN/mm)	Flexural Stiffness Kf (kN/mm)	Kc/Kf
NRC-0	93.2	-	-
FRC-0	166.7	-	-
NRC-30	76.5	45.8	1.67
FRC-30	90.8	48.7	1.87
NRC-60	9.1	6.8	1.34
FRC-60	11	7.9	1.39
NRC-90	4.4	2.7	1.63
FRC-90	4.8	3	1.6
NRC-B	-	7.1	-
FRC-B	-	7.3	-

3.3. Capacity Evaluation

The objective of this section was to evaluate the capacity of the SFRC columns based on the existing knowledge in order for the results to be used in the design and analysis of SFRC columns. In Table 9, the experimental results obtained for each specimen are presented. For the completeness of discussion, the tested flexural specimens are included in Table 9. The maximum axial loads experienced by each straight column are 137 and 187 kN for NRC-0 and FRC-0 columns, respectively, while the maximum calculated ultimate loads using ACI 318 code [22] (Equation (3)) are 151 kN and 176 kN, respectively:

$$P_o = 0.85 \, f'_c \, A_c + f_y \, A_{st} \tag{3}$$

where A_c is the total concrete area; A_{st} is the total steel area. Therefore, the maximum experimental load ratio divided by calculated loads is 0.9 and 1.1 for NRC and FRC, respectively. It should be noted that the corresponding steel fiber in the concrete mixture increases the ratio. The performance of the FRC columns was slightly influenced by the fiber confinement along with transverse steel bars. At the deformation level, the concrete columns reached the yield point, accompanied by separation and micro-cracks in the concrete cover. For the FRC-0 column, the axial load was raised by 12% of the yield load to reach a maximum ultimate load, while there was no increase in the NRC-0. The passive confinement pressure considerably improves at this stage for the FRC column due to the fiber bridging effect that holds the lateral concrete expansion. Therefore, the concrete core of the FRC-0 column gains in strength; at the same time, the cover slowly shows fine cracks. Then, the core reaches the maximum strength, which is the ultimate peak load. Once again, the ultimate load of the FRC-0 column was higher than the load of the NRC-0 column. Therefore, more investigation is recommended to obtain an accurate strength equation for FRC columns.

Table 9. Summary of compressive strength, ductility, and stiffness for all specimens.

Specimen ID	Yield Load (kN)	Vertical Deflection to Yield Load (mm)	Ultimate Load (kN)	Vertical Deflection to Ultimate Load (mm)	Relative Displacement at Ultimate Load (mm)	Horizontal Displacement at Ultimate Load (mm)	Compression Stiffness Kc (kN/mm)	Flexural Stiffness Kf (kN/mm)
NRC-0	137	3.9	137	3.9	-	-	93.2	-
FRC-0	165	2.92	187	11.2	-	-	166.7	-
NRC-30	125	2.2	220	11	1.95	5.02	76.5	45.8
FRC-30	135	2.5	272	12.9	3.72	7.45	90.8	48.7
NRC-60	48	7.2	70	14	4.8	10.32	9.1	6.8
FRC-60	59	6.8	86	13.15	5.32	12.3	11	7.9
NRC-90	19	6.3	25	10.3	3.1	5.1	4.4	2.7
FRC-90	21.5	7.5	30	11.5	2.45	3.85	4.8	3
NRC-B	22	7.9	29	14	-	-	-	7.1
FRC-B	28	6.86	34	15.9	-	-	-	7.3

Based on the limited testing of the V-shape columns with MSSFs, a more detailed evaluation of the tested specimen capacity from the present research is needed. Figure 19 demonstrates the comparisons of percentage increase in the ultimate loads of FRC specimens compared to the corresponding NRC specimens. The comparisons of axial behavior between the vertical and V-shape columns are derived from Figures 8 and 13. Figure 20a shows the deflection at ultimate load for the NSC and FRC specimens, while Figure 20b depicts the relative displacement and horizontal displacement at ultimate load. Figure 19 highlights the benefit of the addition of 1% MSSFs to the concrete mixture to improve the axial strength of the FRC columns. The maximum percentage increase is about 36.5% for the vertical column, while, for all V-shape columns, the percentage increase ranged from 20% to 23.5%, and to 17% for the beam. This improvement in the strength behavior of the FRC specimens is credited to the use of the fiber, which bridges the propagated cracks. Moreover, there were limited differences between FRC and NRC specimens regarding deflections at ultimate load. Therefore, the fiber-bridging effect has a reduced impact on the deflections at ultimate load, while it significantly improves the ductility index and energy absorption of the column. From Figure 20, the angle between columns was found to have a significant influence on deformation behavior. As the angle of the V-shape column increased, the specimens exhibited increased lateral deformation with the increased load. However, with the 90° angle, the deformation was limited due to its low ultimate capacity. A minor increase is visible for a 90° angle due to the inclination of the horizontal load along the column axis. The steel closed stirrups, along with the MSSFs at the base, appear to prevent tension failure at the base compared to NRC specimens. Therefore, due to the significant influence of MSSFs on the axial performance of V-shape columns, the use of MSSFs is recommended with the NSC. Further investigation is also recommended to obtain an accurate strength equation for FRC columns.
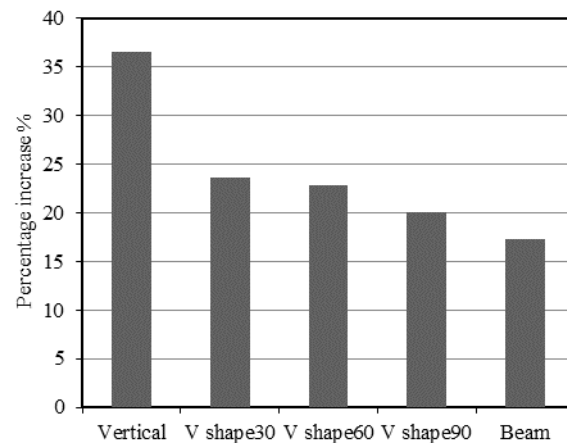
Figure 19. Percentage increase in the ultimate loads of FRC specimens compared to the corresponding NRC specimens.

### 3.4. Experimental Interaction Diagram (P–M Diagram)

A normalized axial load–bending moment curve (P–M curve) was presented based on the experimental calculations for both NRC and SFRC columns to understand the relationship between the angle of inclination and capacity, as summarized in Table 9. The ultimate axial loads and bending moments of the tested vertical columns, V-shaped columns (30°, 60°, and 90°), and flexural beams were utilized to assemble the interaction of the P–M curve, as shown in Figure 21. The interaction curve was assembled from five points. The 1st point indicates the ultimate axial load achieved from the vertical columns tested under loading. The 2nd–4th points indicate the ultimate axial loads and moments attained from the V-shaped columns. The 5th point indicates the ultimate bending moment corresponding to the ultimate flexural load found from the horizontal beams tested under

flexural loading. The ultimate moment of the V-shaped columns of (30°, 60°, and 90°) for the 2nd–4th points in the P–M interaction curve was calculated as follows

$$Mu = Pu\left(\frac{X}{2} + \delta\ horizontal\right) \tag{4}$$

where *Mu* is the ultimate moment matching the ultimate axial load, *Pu* is the ultimate axial load of V-shaped specimen divided by two, *X* is the internal distance between two legs of V-shaped column at free ends, and *δ horizontal* is the ultimate horizontal deformation at the ultimate load. To normalize the ultimate axial loads, the ultimate axial load of all specimens (vertical and V-shaped columns) was divided by the ultimate axial load of the NRC column tested under load. For the V-shaped columns, the ultimate load was divided by two to obtain the ultimate load capacity of a single column. To normalize ultimate moments, the ultimate moment of all specimens (horizontal and V-shaped specimens) was divided by the ultimate moment capacity of the NRC beam under flexural load. The addition of MSSFs in the specimens significantly improved the ultimate axial load and the bending moment compared to the reference specimens with the NRC. The SFRC vertical column specimen demonstrated the highest increase in axial load, and the other SFRC V-shaped and flexural specimens showed a minor increase compared to the NRC specimens.
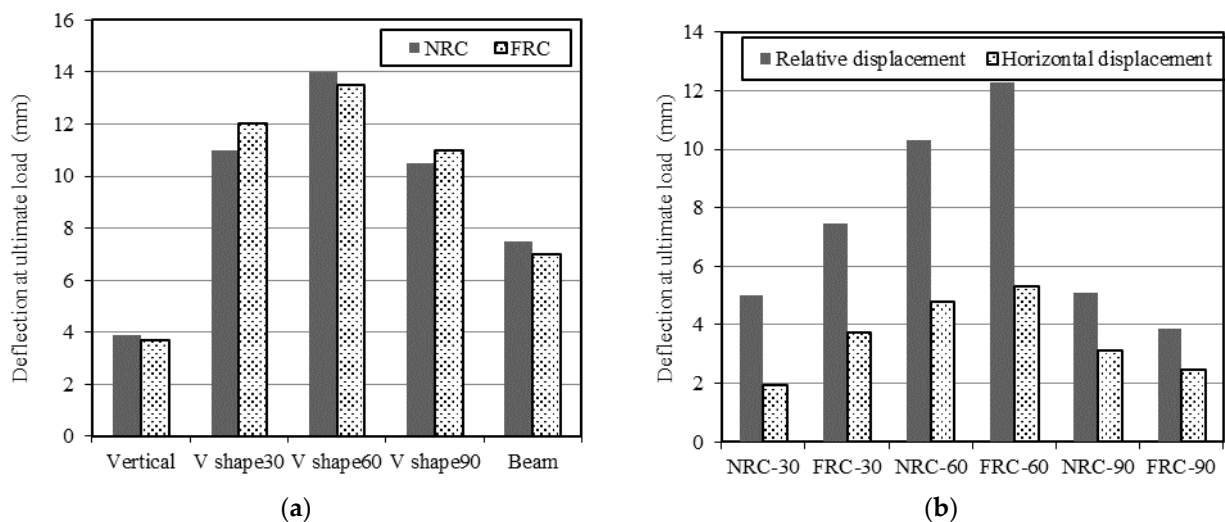
Figure 20. (**a**) Deflection at ultimate load for the NSC and FRC specimens; (**b**) relative displacement and horizontal displacement at ultimate load.
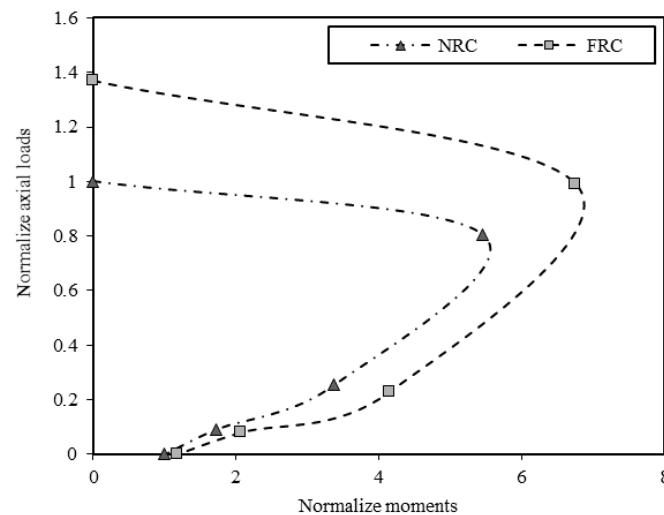
Figure 21. Normalized experimental (P–M) interaction curve.

4. Conclusions

This research focuses on the behavior of V-shaped MSSF-reinforced concrete columns, reinforced with three angles between columns (30°, 60°, and 90°). Along with V-shaped column specimens, two straight columns and two beams were also tested to study the impact of MSSF on axial compression and flexural behaviors. Based on these results, the following conclusions were drawn:

1. The addition of the MSSFs to concrete mix influences the post-ultimate-load behavior of the specimen tested under a concentric load by softening the descending part of the load–vertical displacement curve and avoiding sudden failure.
2. The increase in ductility index due to the addition of MSSF was 79%, and the energy absorption increased by 78%. Thus, the addition of the MSSFs to treat the brittle matter in the specimens under concentric load was very successful.
3. Adding MSSF results in an increment in bending capacity of 17% compared with the NRC beam. Adding MSSF to the flexural beams softened the descending part of the load–midspan displacement curve with an increment in ductility index by 9% and the energy absorption λ by 7%.
4. The V-shaped column with 30°, regardless of the concrete type (with and without MSSFs), exhibited crushing at legends when the sample reached the ultimate load.
5. With an increasing angle of inclination in the V-shaped columns, the ultimate load capacity was decreased by 24%, 23%, and 20% for V-shaped columns with 30°, 60°, and 90° angles of inclination, respectively.
6. All SFRC V-shaped columns showed increased relative and horizontal displacements at ultimate load, except the FRC-90 column. This singular behavior resulted from the main cracks of the FRC-90 column, which were vertical on the inclined leg, while for the other V-shaped columns, the main crack was vertical on the horizontal plane.
7. The increase of 79% in compressive stiffness was observed from the vertical columns, while the compressive stiffness of the V-shaped columns with 30° and 60° angles of inclination amounted to 19% compared to the NRC specimens. The V-shaped column with a 90° angle showed the lowest percent increase in compression stiffness, of about 9.1%.
8. For the deflection at ultimate load for the NSC and FRC specimens, the maximum percentage increase was about 36.5% for the vertical column, while for all V-shape columns, the percentage increase ranged from 20% to 23.5%, and to 17% for the beam. As the angle of the V-shape column increased, the specimens exhibited increased lateral deformation with the increased load. Therefore, the angle between columns significantly influenced the deformation behavior.

The addition of the MSSFs in the samples significantly improved the ultimate load and the bending moment compared to the reference specimens with the NRC. The SFRC vertical column specimen demonstrated the highest increase in axial load, and the other SFRC V-shaped and flexural specimens showed a minor increase compared to the NRC specimens. Other support conditions should be investigated for future research, such as restrained tips (pinned and fixed) at the ends of the inclined legs. Based on the limited testing of the V-shape columns with MSSFs and codes or standards, further investigation is recommended to obtain accurate design equations for FRC straight and V-shape columns.

Data Availability Statement: The data presented in this study are available on request from the corresponding author.

Conflicts of Interest: The authors declare no conflict of interest.

References

1. Lomiento, G.; Bonessio, N.; Benzoni, G.; Phillippi, D.; Hegemier, G.A. Capacity Assessment of V-Shaped RC Bridge Bents. *J. Bridg. Eng.* **2014**, *19*, 266–280. [CrossRef]
2. Phillippi, D.J.; Hegemier, G.A. Shear Loading in Two-Column Bridge Bents. *ACI Struct. J.* **2014**, *111*, 1497–1508. [CrossRef]
3. Phillippi, D.J.; Hegemier, G.A. Simplified Two-Column Analytically Based Fiber Model. *ACI Struct. J.* **2017**, *114*, 349–359. [CrossRef]
4. Eid, R.; Cohen, A.; Guma, R.; Ifrach, E.; Levi, N.; Zvi, A. High-Strength Concrete Circular Columns with TRC-TSR Dual Internal Confinement. *Buildings* **2019**, *9*, 218. [CrossRef]
5. Kytinou, V.K.; Chalioris, C.E.; Karayannis, C.G.; Elenas, A. Effect of Steel Fibers on the Hysteretic Performance of Concrete Beams with Steel Reinforcement—Tests and Analysis. *Materials* **2020**, *13*, 2923. [CrossRef]
6. Gribniak, V.; Kaklauskas, G.; Torres, L.; Daniunas, A.; Timinskas, E.; Gudonis, E. Comparative analysis of deformations and tension-stiffening in concrete beams reinforced with GFRP or steel bars and fibers. *Comp. Part B Eng.* **2013**, *50*, 158–170. [CrossRef]
7. Wang, Z.; Wu, J.; Wang, J. Experimental and numerical analysis on effect of fibre aspect ratio on mechanical properties of SRFC. *Constr. Build. Mater.* **2010**, *24*, 559–565. [CrossRef]
8. Toma, A.; Stanila, A.; Stanila, O. The V-shaped Columns. *Bul. Ştiinţ. Univ. Politeh. Timiş.* **2013**, *58*, 75–78.
9. Chalangaran, N.; Farzampour, A.; Paslar, N. Nano Silica and Metakaolin Effects on the Behavior of Concrete Containing Rubber Crumbs. *CivilEng* **2020**, *1*, 17. [CrossRef]
10. Farzampour, A. Compressive behavior of concrete under environmental effects. In *Compressive Strength of Concrete*; IntechOpen: Rijeka, Croatia, 2019.
11. Chalangaran, N.; Farzampour, A.; Paslar, N.; Fatemi, H. *Experimental Investigation of Sound Transmission Loss in Concrete Containing Recycled Rubber Crumbs*; Virginia Tech: Blacksburg, VA, USA, 2021.
12. Mansouri, I.; Shahheidari, F.S.; Hashemi, S.M.A.; Farzampour, A. Investigation of steel fiber effects on concrete abrasion resistance. *Adv. Concr. Constr.* **2020**, *9*, 367–374.
13. Farzampour, A. Temperature and humidity effects on behavior of grouts. *Adv. Concr. Constr.* **2017**, *5*, 659.
14. Azzawi, R.; Abolmaail, A. Experimental investigation of steel fiber RC hollow columns under eccentric loading. *Structures* **2020**, *24*, 456–463. [CrossRef]
15. Ikponmwosa, E.E.; Salau, M.A. Effect of Short Steel Fibre Reinforcement on Laterized Concrete Columns. *J. Sustain. Dev.* **2011**, *4*, 1. [CrossRef]
16. Al-Tikrite, A.; Hadi, M. Influence of Steel Fibres on the Behaviour of RPC Circular Columns Under Different Loading Conditions. *Structures* **2018**, *14*, 111–123. [CrossRef]
17. Yia, J.; Lia, J. Experimental and numerical study on seismic response of inclined tower legs of cable-stayed bridges during earthquakes. *Eng. Struct.* **2019**, *183*, 180–194. [CrossRef]
18. Tokgoz, S.; Dundar, C. Tests of eccentrically loaded L-shaped section steel fibre high strength reinforced concrete and composite columns. *Eng. Struct.* **2012**, *38*, 134–141. [CrossRef]
19. Teng, Z.-C.; Zhao, T.-J.; Liu, Y. Analysis of the Seismic Performance of a Two-Span Specially Shaped Column Frame. *Adv. Civ. Eng.* **2019**, *2019*, 1–14. [CrossRef]
20. Wang, T.-C.; Zhang, X.-H. Frame property of unequal storey height with specially shaped columns under cyclic loading. *J. Central South Univ. Technol.* **2010**, *17*, 1364–1369. [CrossRef]
21. Wang, T.C.; Lin, H.; Kang, G. Experiment and nonlinear static analysis of RC special-shaped-column frames. *J. Tianjin Univ. Sci. Technol.* **2006**, *39*, 1457–1464. (In Chinese)
22. American Concrete Institute. *Building Code Requirements for Structural 678 Concrete and Commentary*; ACI 318R-11; American Concrete Institute: Farmington Hills, MI, USA, 2014.
23. Iraqi Standard Specification No. 45. *Aggregate from Natural Sources for Concrete and Construction*; Ministry of Planning, Central Organization for Standardization and Quality Control: Baghdad, Iraq, 1984.
24. Al-Baghdadi, H.; Al-Merib, F.; Ibrahim, A.; Hassan, R.; Hussein, H. Effects of Coarse Aggregate Maximum Size on Synthetic/Steel Fiber Reinforced Concrete Performance with Different Fiber Parameters. *Buildings* **2021**, *11*, 158. [CrossRef]
25. *ASTM A615/A615M-20—Standard Specification for Deformed and Plain Carbon-Steel Bars for Concrete Reinforcement*; ASTM International: West Conshohocken, PA, USA, 2020.
26. EN, B. *BS EN 12390-2:2009, Testing Hardened Concrete. Making and Curing Specimens 673 for Strength Tests*; British Standard; British Standards Institution: London, UK, 2009.
27. *ASTM C496/C496M-17—Standard Test Method for Splitting Tensile Strength of Cylindrical 671 Concrete Specimens*; ASTM International: West Conshohocken, PA, USA, 2017.
28. *ASTM C78/C78M-18—Standard Test Method for Flexural Strength of Concrete (Using 675 Simple Beam with Third-Point Loading)*; ASTM International: West Conshohocken, PA, USA, 2018; Volume 676.

29. Hassan, R.F.; Jaber, M.H.; Al-Salim, N.H.; Hussein, H.H. Experimental research on torsional strength of synthetic/steel fiber-reinforced hollow concrete beam. *Eng. Struct.* **2020**, *220*, 110948. [CrossRef]

30. Han, J.; Zhao, M.; Chen, J.; Lan, X. Effects of steel fiber length and coarse aggregate maximum size on mechanical properties of steel fiber reinforced concrete. *Constr. Build. Mater.* **2019**, *209*, 577–591. [CrossRef]

31. Al Rikabi, F.T.; Sargand, S.M.; Khoury, I.; Hussein, H.H. Material Properties of Synthetic Fiber–Reinforced Concrete under Freeze-Thaw Conditions. *J. Mater. Civ. Eng.* **2018**, *30*, 4018090. [CrossRef]

32. ASTM International. *C192/C192M-13a-Standard Practice for Making and Curing Concrete Test Specimens in the Laboratory*; Technical Report; ASTM International: West Conshohocken, PA, USA, 2013.

33. Hadi, M.N.; Khan, Q.S.; Sheikh, M.N. Axial and flexural behavior of unreinforced and FRP bar reinforced circular concrete filled FRP tube columns. *Constr. Build. Mater.* **2016**, *122*, 43–53. [CrossRef]

34. Hadi, M. Behaviour of eccentric loading of FRP confined fibre steel reinforced concrete columns. *Constr. Build. Mater.* **2009**, *23*, 1102–1108. [CrossRef]

35. Koçera, M.; Öztürk, M.; Arslana, H. Determination of moment, shear and ductility capacities of spiral columns using an artificial neural network. *J. Build. Eng.* **2019**, *26*, 100878. [CrossRef]

36. Pessiki, S.; Pieroni, A. Axial load behavior of large-scale spirally-reinforced highstrength concrete columns. *ACI Struct. J.* **1997**, *94*, 304–314.

37. Saljoughian, A.; Mostofinejad, D. Corner Strip-Batten Technique for FRP-Confinement of Square RC Columns under Eccentric Loading. *J. Compos. Constr.* **2016**, *20*, 4015077. [CrossRef]

38. Huo, J.; Huang, G.; Xiao, Y. Effects of sustained axial load and cooling phase on post-fire behaviour of concrete-filled steel tubular stub columns. *J. Constr. Steel Res.* **2009**, *65*, 1664–1676. [CrossRef]

39. Yang, Y.-F.; Cao, K.; Wang, T.-Z. Experimental behavior of CFST stub columns after being exposed to freezing and thawing. *Cold Reg. Sci. Technol.* **2013**, *89*, 7–21. [CrossRef]

40. Vu, N.S.; Li, B.; Beyer, K. Effective stiffness of reinforced concrete coupling beams. *Eng. Struct.* **2014**, *76*, 371–382.

41. Bhargava, P.; Sharma, U.K.; Kaushik, S.K. Compressive Stress-Strain Behavior of Small Scale Steel Fibre Reinforced High Strength Concrete Cylinders. *J. Adv. Concr. Technol.* **2006**, *4*, 109–121. [CrossRef]

42. Liao, W.-C.; Perceka, W.; Liu, E.-J. Compressive Stress-Strain Relationship of High Strength Steel Fiber Reinforced Concrete. *J. Adv. Concr. Technol.* **2015**, *13*, 379–392. [CrossRef]